Impact of CO_2 Injection in Deep Saline Aquifers: A study on Pressure Evolution in Stratified Formation of Qianjiang sag, China

Telesphore Kabera and Yilian Li

***Abstract*— In order to mitigate the adverse impacts of climate change, CO_2 captured from carbon emitters like coal-fired power plants may be stored in deep saline aquifers. This action may cause pressure changes, which affect subsurface volumes. The main purpose of this study is to evaluate the pressure changes during CO_2 sequestration in CO_2 storage formation embedded in a sequence of aquifers and aquitard of the Qianjiang depression area. In order to demonstrate the transient pressure, we have conducted TOUGH2 modeling of CO_2 injection into closed formations of different thicknesses assuming impermeable boundaries. A 2-D radially symmetric model was developed to represent a CO_2 storage site in the Qianjiang depression area. The storage formation into which CO_2 is injected is 120 m thick and located at a depth of about 1530 m below the ground surface. The CO_2 injection thickness was 25m from the bottom of the storage formation. Carbon dioxide is injected into a zone of 71 m radial extent representing a few distributed wells. Injection occurs at an annual rate of 1* 10 7 tonnes of CO_2 representing six times the CO_2 rate captured from a medium-size-coal-fired power plant. The simulation runs cover a time period of 100 years altogether, comprising the 20-year injection period and 80-year post-injection period. Our simulation results indicate that interlayer pressure propagation through a sequence of aquitard/aquifer will not affect the top aquifer except for the case when seal permeability was 9 * 10-18 m2, after 100 years the pressure perturbation reached the upmost aquifer .Placing a barrier (fault) at a distance of 10 km have shown that the flow barrier started affecting pressures after about 1 month and 24 days and the pressure increase were very high, about 150 bars after 20 years.**

***Index Terms*—Aquitard/Aquifer, Depression area , Pressure Buildup, Qianjiang, TOUGH2.**

I. Introduction

Geologic carbon sequestration in deep formation has drawn increasing consideration as a promising method in order to mitigate the adverse impacts of climate change [1]; [2]; [3] and [4].

Generally, CO_2 sequestration is defined as the removal of gas that would be emitted into the atmosphere and its subsequent storage in a safe, sound place [5].

The implementation of worldwide ongoing and former projects such as natural gas processing at Sleipner in the North Sea [6], at Salah in Algeria [7], enhanced oil recovery at Weyburn in Canada [8], Nagakoa pilot project in Japan [9] and the Frio brine project in Texas [10] demonstrate the feasibility of injecting CO_2 into subsurface geological reservoirs.

Once the CO_2 is injected into pore spaces of the storage aquifer, it displaces much of the in situ pore-water. This process causes a progressive increase in formation fluid pressure, centered on the injection point and exacerbated by high injection rates, low reservoir permeability, and the presence of barriers to fluid flow, such as fault. Pressure increase will limit the rate at which CO_2 can be injected, and ultimately may limit the amount of CO_2 that can be practically stored [11].

Reservoir injectivity is defined as the capacity of a reservoir to accept injected CO_2 at a specified rate and for the required cumulative amount.

In regard to pressure changes within the storage formation, the region of influence in response to CO_2 injection can be extremely large [11]. Zhou et al. [12] suggested that the hydraulic characteristics of seal layers may strongly affect the lateral and vertical volumes affected by pressure buildup. Normally suitable sites for CO2 sequestration would typically have thick, laterally continuous shale, mudstone, or siltstone seals that act as permeability and capillary barriers to impend or prevent upward migration of buoyant CO_2 [11].

Data used during the present research are from the Wangchang oil field. The Wangchang oil field is located in the northern part of Qianjiang depression area where the Qianjiang depression covers 2500 km^2 and it has most of the current petroleum production [13]. The rock type in the study area consists mainly of feldspar quartz sandstone and quartz sandstone debris, in addition to small amounts of feldspar sandstone and feldspar lithic sandstone. Quartz content is generally 60 to 90%, Feldspar content occupies about 5 to 25% and debris content of about 5 to 15 % mainly in acid volcanic rocks [14].

The main aim of this research is the demonstration of pressure change during CO_2 injection in CO_2 storage formation embedded in a sequence of aquifers and aquitard of the Qianjiang depression area.

In order to demonstrate the transient pressure, we have conducted TOUGH2 modeling of CO_2 injection into closed formations of different thicknesses assuming impermeable boundaries. The whole work was done using the TOUGH2/ECO2N simulator [15],[16]. ECO2N module includes a comprehensive description of the thermodynamics and thermophysical properties of H_2O-NaCl-CO_2 mixtures. It is designed to reproduce fluid properties to within experimental error for temperature in the range 10 to 110 0C, for pressure up to 60 MPa, and for salinities up to full halite saturation.

II. Conceptual Model and Model Setup

A 2-D radially symmetric model was developed to represent a CO_2 storage site in Qianjiang depression area. The storage formation into which CO_2 is injected is 120 m thick and located at a depth of about 1380 m below the ground surface. The CO_2 injection thickness was 25m from the bottom of the storage formation. The storage formation is bounded at the top by a sealing layer of 30 m (see fig. 1), followed by a sequence of aquifers and sealing layers with various thicknesses. The bottom of the storage formation is formed by a layer considered in the present study as impermeable base rock with thickness of about 100 m. Altogether; the model domain includes four aquifers and five aquitards. The lateral extent boundary is located at 200km, which corresponds to a footprint area of about 125,664 km^2. The large lateral extent was chosen in order to ensure that the boundary condition would have minimal effect on the simulation results.

Carbon dioxide is injected into a zone of 71 m radial extent representing a few distributed wells. Injection occurs at an annual rate of $1 * 10^7$ tonnes of CO_2 representing six times the CO_2 rate captured from a medium-size-coal-fired power plant. The simulation runs cover a time period of 100 years altogether comprising the 20-year injection period and a 80-year post-injection period.

III. Model Parameters

The hydrogeologic properties chosen for the aquifer-aquitard sequence are given in Table 1. For a given porosity, mudstone permeability varies over a range of 2–5 orders of magnitude [17], During our work we have varied seal permeability over a wide range : ks = $9.0 * 10^{-17}$ to $9.0*10^{-22}$ which fall in the range of sealing layers, in the previous research where [11] used shale as sealing layer, the seal permeability was varied over a wide range: ks =$1.0 * 10^{-16}$ to $1.0 * 10^{-21}$ m^2 based on shale permeabilities reported in [18], [19] [20],and Hart et al. [21].

Apart from the seal permeability variations, pore compressibility which is another parameter defining the pressure response to CO_2 injection was considered. In the first case the compressibility values used are the ones presented in Table 1 whereas for the sensitivity analysis cases: firstly the compressibility of all layers is considered to vary linearly with depth, starting with the values given in Table 1 for the deepest aquifer and aquitard, respectively, assuming a one-order-of-magnitude increase over the entire vertical sequence (to account for the fact that shallower units are often less consolidated and thus more compressible than deep units), secondly we have reduced the base-case compressibility values by one order of magnitude and finally it was increased by one order of magnitude. The different cases reflect the range of pore compressibilities measured over a wide range of subsurface materials (e.g., [22], [19], [23],[24]. Note that the compressibility of the fluids (i.e., CO_2 and water) is intrinsically taken into account in TOUGH2/ECO2N in terms of density variations with fluid pressure. The sensitivity cases addressing pore compressibility have all been conducted using a seal permeability of $9*10^{-20}$ m^2 (The seal permeability considered in base case).

In order to investigate the effect that flow compartmentalization (faulting) has on pressure evolution during and subsequent to CO_2 injection, low permeability vertical elements were introduced into the mesh at a distance of 10 km from the injection point.

Fig.2 shows the initial conditions used for the simulations in a vertical profile. There are no lateral variations, meaning that the system is stagnant prior to injection of CO_2, this explains that regional groundwater flow is neglected. Initial pressure is hydrostatic. Temperature varies linearly with depth, within the Qianjiang depression area, in sandstone and mudstone, the gradient is high, 3 to 4^0 C/100m and in salt layers the geothermal gradient is low compared to sandstone and mudstone units. In salt, the geothermal gradient is commonly 2.3 to 3.0^0 C/100 m [26]. Salt mass fraction vertical profile was prepared based on the idea that in Qianjiang depression area, the depth of burial lower than 1250m, water salinity increases with depth; as the burial depth deeper than 1250m, the water salinity varies from 250000 mg/L to 340000 mg/L, and is almost in the saturation state; when the burial depth is deeper than 1650m. The vertical salinity profile represents an equilibrated system where no density-driven flow occurs at the initial state.

IV. Results and Discussion

A. Spatial Distribution of Co_2 Plume

In order to choose safe seal permeability for our study, we focused on the characteristics of the CO_2 plume at the end of the injection period, shown in fig.2. The two first cases difference is only the seal permeability values (for case 1: ks = $9 * 10^{-17}$ m^2 and case 2: ks = $9 *10^{-20}$ m^2) and for case 3 the seal permeability is the same as the 2nd seal permeability value ($9 * 10^{-20}$ m^2) the only difference is the injection rate which was increased from 10 million tones per year to 30 million tones per year.

Fig.2 shows the plume size using saturation contours for supercritical CO_2. The plume in 2nd case (ks = $9*10^{-20}$ m^2) is about 8.5 km and for all cases the plume is concentrated at the top of the storage formation, a result of buoyancy forces. The CO_2 plumes are identical for all seal permeability from ks equal to $9 * 10^{-20}$ m^2 and below (only 3 cases are shown here for brevity). When the seal permeability is grater than $9 * 10^{-20}$ m^2 the CO_2 plume migrates into the sealing unit immediately above the storage formation (Aquifer 1) after 20 years of injection, indicating that CO_2 may not be safely trapped over longer time periods. When the CO_2 injection rate was increased from 10 million tones to 30 million tones (ks is equal to $9 * 10^{-20}$) the CO_2 plume was extended to about 10 km laterally and remains safe because it does not migrate into sealing unit above the storage reservoir.

B. Lateral and Vertical Pressure Buildup

In this section, we evaluate the pressure perturbation in the subsurface in response to CO_2 injection using different seal permeabilities in different times (after 1 year, 20 years of injection and 80 years after the end of CO_2 injection), notice that for the same time different seal permeabilities are used, we have varied seal permeability as follows: case 1: ks = 9 *

10^{-18} m^2, case 2 : ks = 9 * 10^{-20} m^2 and case 3: ks = 9 * 10^{-22} m^2 (Corresponding to hydraulic conductivities 0.009119 millidarcy, 0.00009119 millidarcy and 0.0000009119 millidarcy. Notice that a cutoff value of 0.1 bar is set for the contours; meaning that the pressure buildup less than 0.1 bar, or less than a 1 m increase in groundwater elevation , is not colored.

It is evident from fig.3 that the permeability of the sealing layers has a strong effect on both the vertical and the horizontal pressure propagation. After 1 year injection, the case 2 (when the seal permeability is 9*10^{-20} m^2) shows a pressure increase of 0.1 bar extending almost 60 km laterally within the storage formation, corresponding to an area of influence covering about 11309.7 km^2 whereas at the end of injection (fig.3 (b)) the pressure increase of 0.5 bar occupies the whole laterally distance within the storage formation. This area is very large compared to the CO_2 plume of 8.5 km (fig.3). When the seal permeability is increased by 2 order of magnitude (ks = 9 * $10^{-18}$$m^2$), a different behavior occurs, the area of influence becomes about 6082 km^2. The pressure propagation upward from the storage formation is significant, notice that the maximum near the injection zone is reduced as apparent from pressure increases extending all the way to a depth of about 100 m from the top of the top unit (aquitard 1) (fig.3 (a)) affecting aquifer 2 and 3. For other two cases (ks = 9 * 10^{-20} and 9 * 10^{-22} m^2) the upward pressure increase propagation does not reach aquifer 2. It only affects the storage aquifer. When seal permeability is high, brine leakage resulting from interlayer communication has a positive attenuation effect on the pressure conditions within the storage formation, while allowing for vertical pressure propagation that may reach shallow aquifers as indicated by [11].

A 2-bar pressure buildup (equal to 20 m increase in piezometric head), is observed at 16 km (when ks = 9 * 10^{-18} m^2), 24 km (when ks = 9 * 10^{-20} m^2), and 32 km (when ks = 9 * 10^{-22} m^2) at the end of injection period (after 20 years) whereas after 1 year injection period it is observed at 12 km (when ks = 9 * 10^{-18} m^2), 18 km (when ks = 9 * 10^{-20} m^2), and 18 km with few meters (when ks = 9 * 10^{-22} m^2).

Assuming having a gently updipping formation that forms a confined aquifer freshwater aquifer at 24 km radial extent (instead of the horizontal stratigraphy used in the present study). Ignoring the impact of vertical variations and compressibility, the shallow groundwater resource would experience a piozometric head change of about 20 m. Notice that at the end of injection period (when ks is equal to 9 * 10^{-20} m^2), a different behavior occurs the pressure propagation upward from the storage formation has reached the aquitard 3.

Fig.3 .c shows the pressure buildup for the same three cases during the post-injection period, 80 years (after injection stops). Compared to fig.3.b, the pressure perturbations have relaxed significantly, with maximum pressure increases not more than 0.6 bars. However, as maximum pressure tends to return to an equilibrium state, the area of influence widens considerably. In case of ks = 9 * 10^{-18} m^2, a pressure increases of less than 0.2 and greater than 0.1 bar is occupying the whole storage lateral distance except near the injection zone where the pressure increases is 0.1 bar up to 110 m from the bottom of the storage formation while, on the other hand, shows that the pressure perturbation can reach the upmost aquifer , with the same pressure increases as in lateral direction and it corresponds to a change of about 2 m in the groundwater piezometric surface of the confined aquifer.

Fig.3 shows the contours of pressure change in two different stratigraphic units: in the storage formation and in the top aquifer. Results are presented for four seal permeabilities from 9*10^{-22} m^2 to 9*10^{-17} m^2 at different lateral distances (i.e., R = 10.24, 29.96 km and 69.97 km) from the injection zone. The transient pressure buildup in the storage formation (fig.4.a) is significantly affected by both radial location and seal permeability. Pressure buildup is larger close to the injection zone (fig.4.a). At larger Radius, the pressure buildup is small and occurs later. The fig. 4 shows that for R1 the pressure response happens directly when CO_2 is injected into the storage formation whereas for R3 it takes sometime to happen. The maximum pressure closer to the injection zone (10.24 km) is observed after about 6years whereas for far away from the injection zone (R3 = 69.97 km) the maximum pressure is observed after 20 years (the time injection stops). For all considered cases the maximum pressure has been reached before the injection ceases except for the highest radial distance (R3 = 69.97 km) where the maximum pressure was reached at the time the injection stops (20 years), signaling that hydrological system to reclaim a complete system has been reached.

Concerning the impact of seal permeability, from the observed behavior, two cases (ks equal to 9*10^{-20} m^2 and 9*10^{-22} m^2) make aquitards look like impermeable seals; these cases show the strongest pressure perturbation in the storage formation. Notice that for other cases considered in the present study (9*10^{-17} m^2 and 9*10^{-18} m^2) Show moderate/drastic reduction in the maximum pressure – about 79% in the 9*10^{-17} m^2 case, 30 % in the 9*10^{-18} m^2 case (based on the 10.24 km radial extent graph), this demonstrate the importance of interlayer brine flow.

The top row of plots in fig.4 shows pressure evolution in aquifer 4, which is the uppermost aquifer and it is separated from the storage formation by three sealing layers. Over 100 years of simulation period, pressure impacts are observed only in the two cases with high seal permeabilities (9*10^{-17} m^2 and 9*10^{-18} m^2), the magnitude of pressure buildup depending on the radial location and the seal permeability. The maximum pressure increase-about 3.15 and 1.55 bar, respectively at R=10.24 km whereas in storage formation they are 4 and 5.5 bar, respectively. The pressure increase values obtained in the upmost aquifer (3.15 and 1.55 bar) correspond to changes in piezometric head of 31.5 and 15.5 m, respectively.

C. Pore Compressibility Effect on Pressure

As shown above the safe seal permeability in the present study was found to be 9 * 10^{-20} m^2, therefore it is used as a starting point, the following additional simulations runs were performed as follows: (1) the pore compressibility of all layers is considered to vary linearly with depth, starting with values given in Table 1 for the deepest aquitard and aquifer, respectively, and assuming a one-order-of-magnitude

increase over the entire vertical sequence, (2) the pore compressibility in all layers is increased by one-order-of magnitude, and finally (3) the pore compressibility in all layers is reduced by one order of magnitude.

Results are shown in fig.5, in that figure the vertical pressure profiles at radial extents 10.24 and 29.96 km, for the different sensitivity cases, after 1 of the injection period, at the end of the injection period of 20 years and at 80 years after the injection ceases. From the results (Fig.5), considering the pore compressibility to vary linearly with depth has minor effects on the pressure results in comparison with the base case, this is due to the fact that the largest compressibility differences are in the uppermost layers where the pressure impact of CO_2 injection is very small. In the two other cases the results obtained are different from the base case results:

reducing the pore compressibility in all layers by one-order-of magnitude causes a higher pressure buildup in the storage formation, as well as a large region of influence, in both the lateral and the vertical direction except in the one case (at R1 at the end of the injection period (after 20 years)) where the results are almost similar to the base case results in the storage formation. At 100 years, pressure changes propagate up to the top aquifer.

Increasing the pore compressibility in all layers by one-order-of magnitude, the magnitude and spatial extent of pressure build up is smaller than in the base case. The exception is the pressure response in the overlying aquitard (Aquitard 2) during the post-injection period at 100 years. Notice that during the post-injection period the pressure change results from the base case propagate up to the top aquifer.

The pressure values at 10 km are the highest of all cases, caused by the increase in compressibility and resultant reduction in hydraulic diffusivity, defined by $k/\Phi\rho_w\mu_w(\beta_w + \beta_p)$, where k is permeability and μ_w is water viscosity [11].

D. Flow Barrier

Due to the presence of fault in Qianjiang depression area, one simulation was performed in which we set the barrier at a distance of 10 km from the injection point, making the area of injection 314 km^2. The CO_2 injection lasts for 20 years. The flow barrier was assigned the same permeability as the sealing units (9 * 10-20 m^2). Fig. 7 shows the results obtained for two radiuses (at 1.024 and 9.981 km).

V. Conclusion

Through numerical modeling of the Qianjiang depression area subsurface formations with a single injection zone, we have demonstrated pressure response to the CO_2 injection in the mentioned formations. The characteristics of pressure buildup and their magnitude depend on the radial location and seal permeability.

Safe seal permeability value for the present study was found to be 9 * 10^{-20} m^2, this seal permeability was used in sensitivity cases about pore compressibility

Considering the pore compressibility to vary linearly with depth has minor effects on the pressure results in comparison with the base case, this is due to the fact that the largest compressibility differences are in the upmost layers where the pressure impact of CO_2 injection is very small. In the two other cases the results obtained are different from the base case results: reducing the pore compressibility in all layers by one-order-of magnitude causes a higher pressure buildup in the storage formation, as well as a large region of influence, in both the lateral and the vertical direction except in the one case (at R1 at the end of the injection period (after 20 years)) where the results are almost similar to the base case results in the storage formation. At 100 years, pressure changes propagate up to the top aquifer.

Increasing the pore compressibility in all layers by one-order-of magnitude, the magnitude and spatial extent of pressure build up was smaller than in the base case. The only exception was the pressure response in the overlying aquitard (Aquitard 2) during the post-injection period at 100 years. It was Noticed that during the post-injection period the pressure change results from the base case propagate up to the top aquifer.

When a barrier (fault) was place at a distance of 10 km have it showed that the flow barrier started affecting pressures after about 1 month and 24 days and the pressure increase is very high, about 150 bars after 20 years.

Appendix

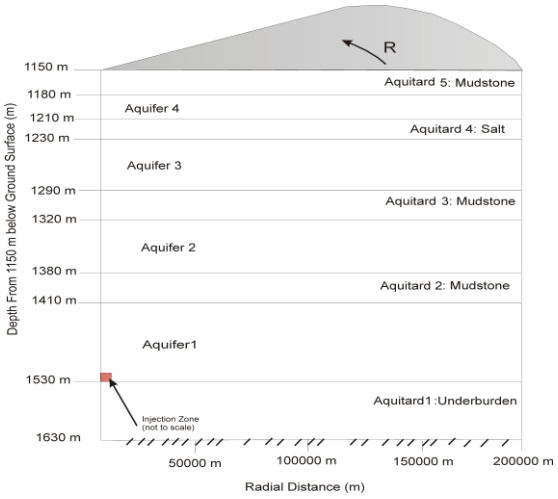

Fig. 1- Schematic showing a vertical cross-section of the radially symmetric model domain with deep brine formation CO_2 storage and overlying aquifer/aquitard sequence.

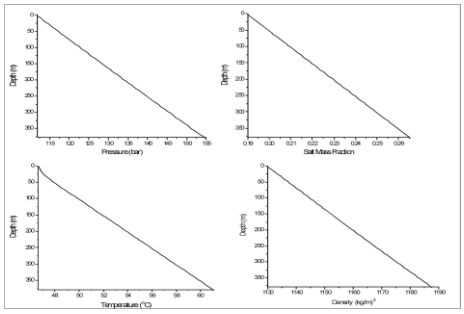

Fig. 2- Vertical Profile of initial pressure, salt mass fraction, temperature and brine density from the top aquifer to the storage formation

TABLE I. THE COMBINATION OF RESERVOIR, COVER LAYER OF QIANJIANG DEPRESSION AREA

System	Series	Formation		Thickness (m)	Lithology Character
Eogene	Oligocene	Qian 1	upper	120 ~ 450	Referred to as "mud-gypsum layer"; consists of gray to dark mudstone, gypsum-mudstone, oil shale with intercalated salt
			Middle		Intercalation of gray mudstone and siltstone
			Lower		Intercalation of gypsum, salt, sandstone and mudstone, with some oolitic marlite
	Eocene	Qian 2		110 ~ 700	Consists of 24 rythmic units, each composed of salt, gypsum-mudstone, glauberite mudstone, oil-bearing mudstone, marlite occasionaly, silty fine-grained sandstone occurs at the bottoms of the units
		Qian 3	Upper	150 ~ 640	Gray to dark-gray mudstone, siltstone and oolitic marlite; three rhythmic units and two suites of sandstone
			Lower		Consists of 14 rhythmic units,each composed of dark-gray mudstone, gypsum mudstone and salt, with some silty fine-grained sandstone
		Qian 4	Upper	100 ~ 700	Gray and dark gray mudstone, glauberite mudstone, salt, oil-bearing mudstone and silty fine-grained sandstone
			Lower	600 ~ 1000	Gray and dark-gray mudstone, glauberite-mudstone, salt, oil-bearing mudstone

TABLE II- Hydrogeological properties used in the base-case simulations

Properties		Aquifer	mudstone	salt
Permeability, k (m^2)	Horizontal	9.0×10^{-13}	9.0×10^{-20}	9.0×10^{-20}
	Vertical	9.0×10^{-13}	9.0×10^{-20}	9.0×10^{-20}
Porosity		0.16	0.10	0.10
Pore compressibility (Pa^{-1})		4.5×10^{-10}	9.0×10^{-10}	
Rock grain density (kg m^{-3})		2600		
Formation heat conductivity under fully liquid-saturated conditions (W/m °C)		2.51		
Rock grain specific heat (J/kg °C)		920		
Temperature (°C)		46		
Pressure (bar)		Refer to the fig.2		
Salinity (mass fraction)		Refer to the fig.2		
k_{rl} : Liquid relative permeability		$k_{rl}=\sqrt{S^*}\left\{1-(1-\left[S^*\right]^{1/m})^m\right\}^2$, $S^*=(S_l-S_{lr})/(1-S_{lr})$		
S_{rl} : Residual water saturation		S_{rl} = 0.20	S_{rl} = 0.20	S_{rl} = 0.20
k_{rg} : Gas relative permeability		$k_{rg}=(1-\hat{S})^2(1-\hat{S}^2)$, $\hat{S}=(S_l-S_{lr})/(S_l-S_{lr}-S_{gr})$		
S_{gr} : Residual gas saturation		S_{gr} = 0.05	S_{gr} = 0.05	S_{gr} = 0.05
P_{cap} : Capirally pressure		$P_{cap}=-P_0(\left[S^*\right]^{-1/m}-1)^{1-m}$, $S^*=(S_l-S_{lr})/(1-S_{lr})$		
m : Van Genuchten		m = 0.46	m = 0.46	m = 0.46

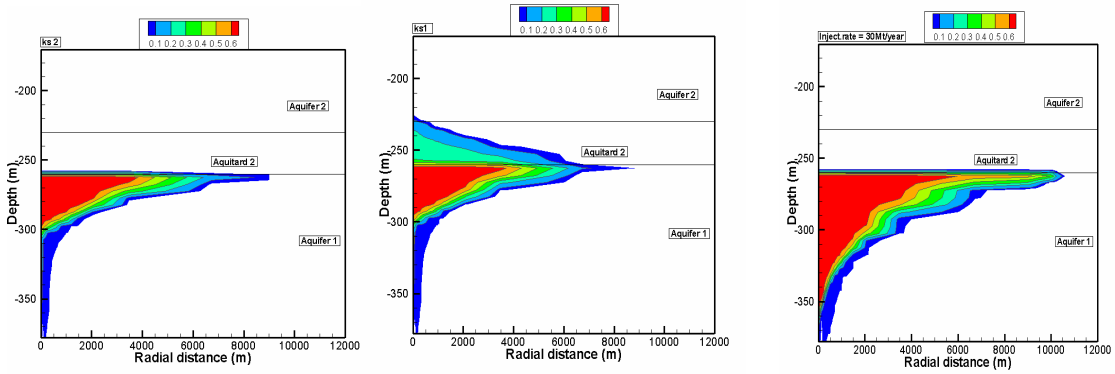

Fig.3- Contours of CO_2 saturation at the end of the injection period (30 years) for different scenarios (case1: ks1 = $9*10^{-17}$, case 3: ks1 = $9*10^{-20}$and case 5: inj.rate = 30Mt per year).

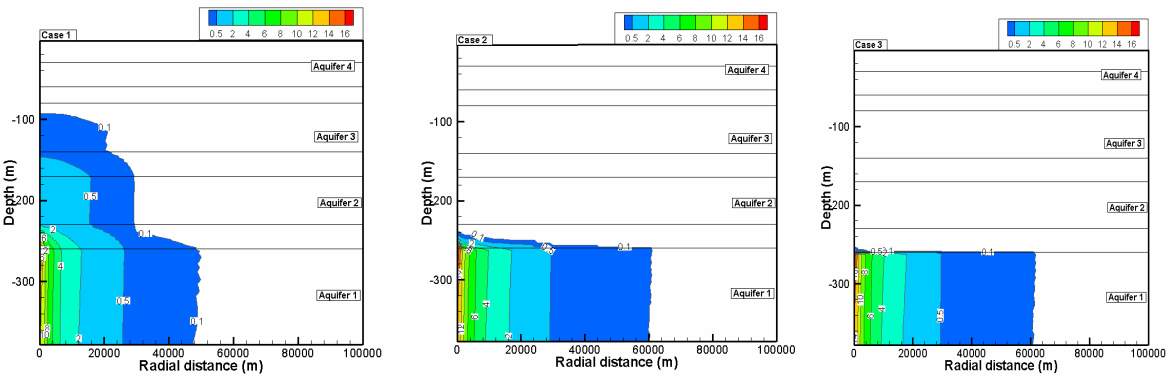

(a) After 1 year injection

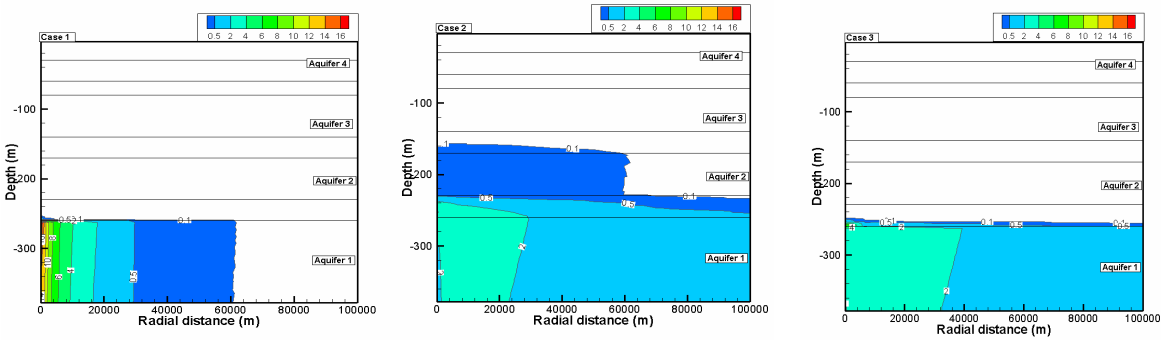

(b) At the end of the injection period (20 years)

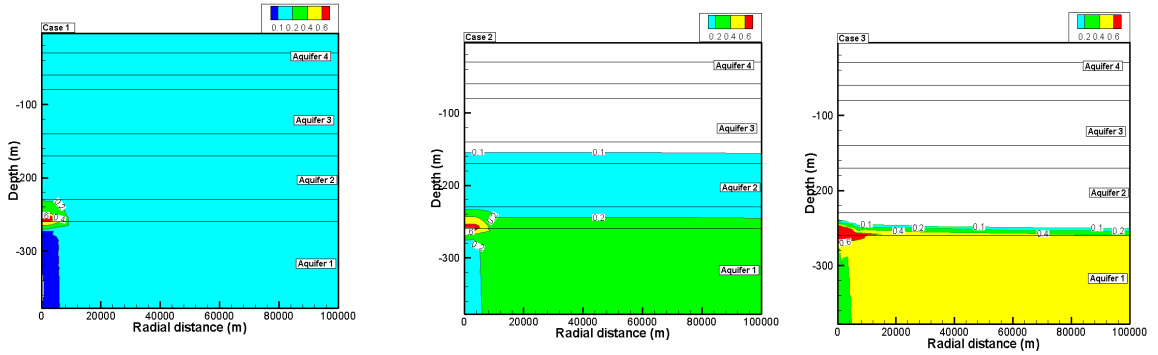

(c) After 80 years injection has ceased

Fig. 4- Contours of pressure buildup (change in fluid pressure from the initial hydrostatic condition) after 1 year (a), 20(b) and 80 years after injection of CO_2 injection and, for different values of seal permeability and different pore compressibility values.

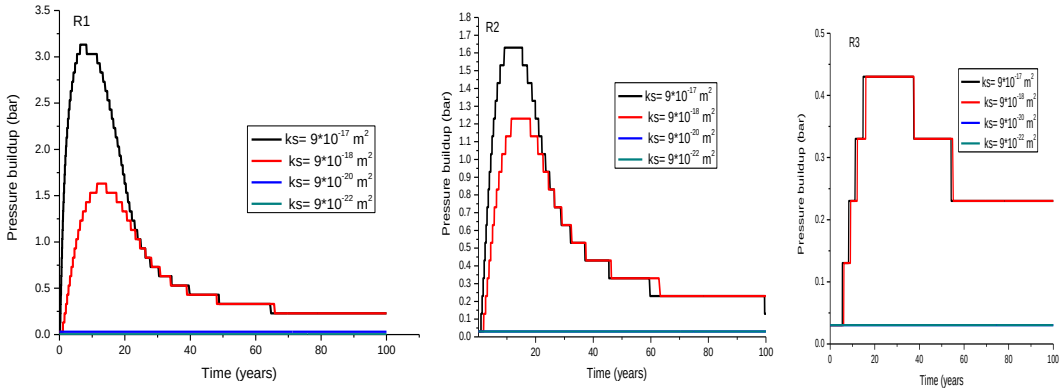

(a)Top aquifer

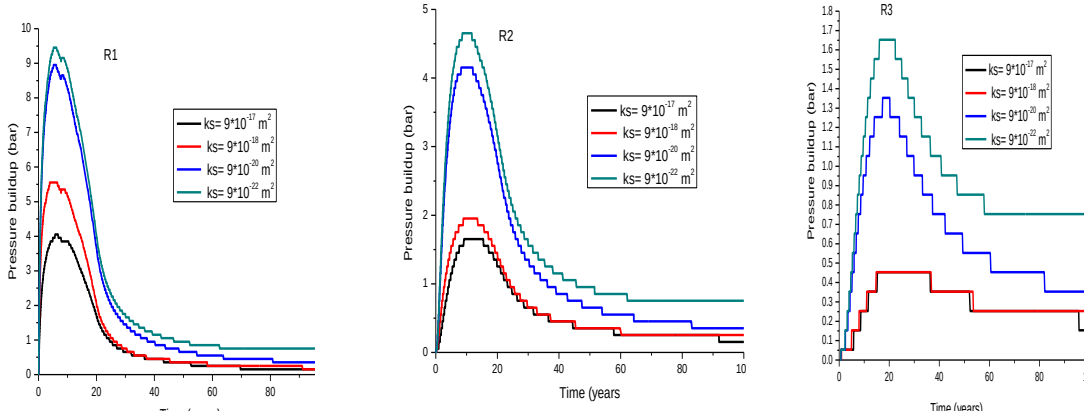

(b) Storage

Fig. 5- Sensitivity of pressure evolution to seal permeability. Pressure results are plotted at different radial locations and in different aquifers (storage formation and the top aquifer.

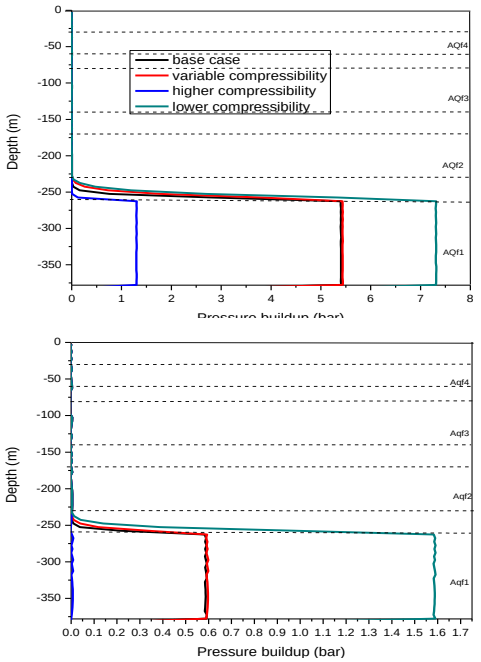

(a) T= 1 year, R1 and R2

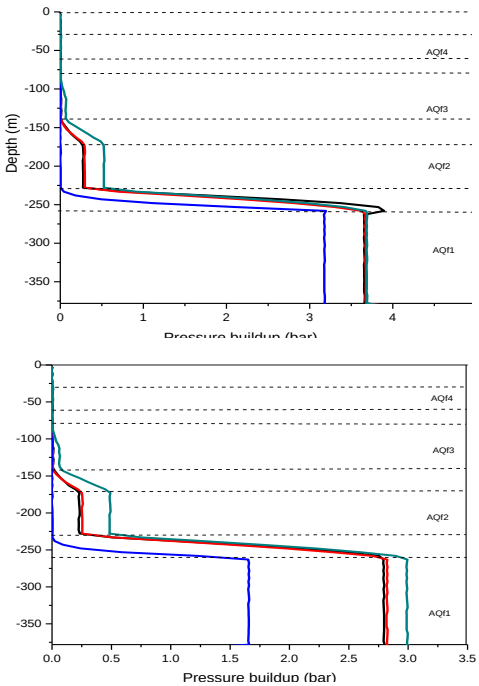

(b) T= 20 years, R1 and R2

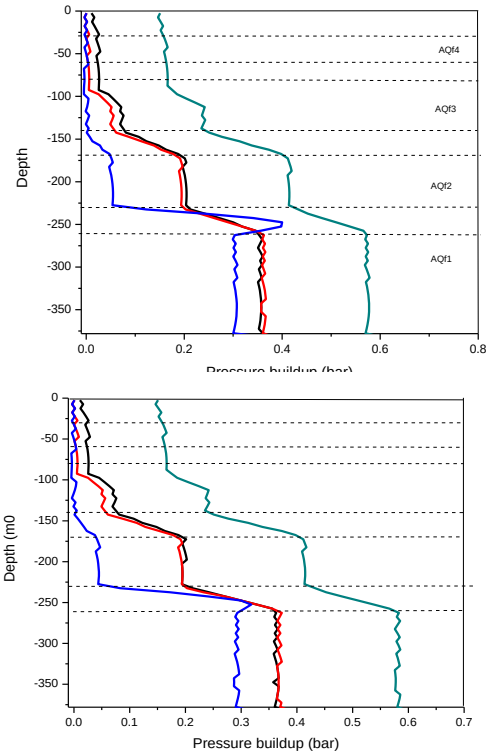

(C) T= 100 years, R1 and R2

Fig. 6- Vertical pressure profiles at 10.24 and 29.96 km radius for 1, 20 and 100 years since the beginning of CO_2 injection, for different compressibility sensitivity cases.

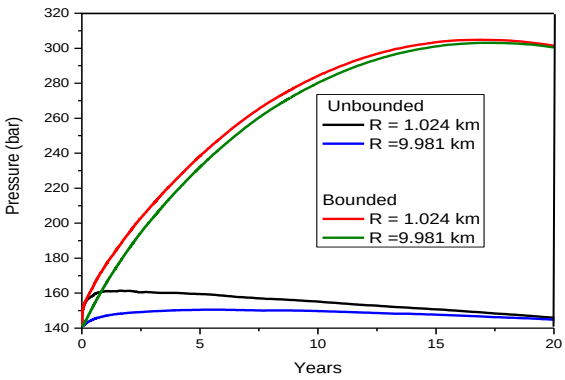

Fig. 7- Calculated pressures for an unbounded Qianjiang model and a model with a barrier (boundary) 10 km from the injection point.

ACKNOWLEDGEMENT

The authors would like to acknowledge helpful comments and discussions from our working group. This work was supported by the National Natural Science Fundation of China (NSFC, Nos. 40472122 and 40672168) and GCEP (subcontract 238463-43106-A).

REFERENCES

[1] Holloway, S., An overview of the Joule II Project: the underground disposal of carbon dioxide. Energy Convers. Manage. 37 (6–8), 1996, 1149–1154

[2] Gale, J., Geological storage of CO_2: what do we know, where are the gaps, and what more needs to be done? Energy 29 (9–10), 2004, 1329–1338.

[3] IPCC (Intergovernmental Panel on Climate Change), 2005. IPCC Special Report on Carbon Dioxide Capture and Storage.

[4] Hepple, R.P., Benson, S.M., Geologic storage of carbon dioxide as a climate change mitigation strategy: performance requirements and the implications of surface seepage. Environ. Geol. 47, 2005, 576–585. Cambridge University Press, New York.

[5] Dai, S.Z., China Petroleum Geology Record, vol. 9.,1991, Petroleum Industry Press, Jianghan Oilfield, Beijing (in Chinese).

[6] Baklid, A., Korbøl, R. & Owren, G, Sleipner Vest CO_2 disposal, CO2 injection into a shallow underground aquifer. Paper SPE 36600, presented at the SPE Annual Technical Conference and Exhibition, 6–9 October, 1996, Denver Colorado, USA.

[7] Riddiford, F.A., Tourqui, A., Bishop, C.D., Taylor, B. & Smith, M, A cleaner development: the In Salah Gas project, Algeria. In: Gale, J. & Kaya, Y. (eds) Greenhouse Gas Control Technologies. Pergamon, Amsterdam, 2003, 595–600.

[8] Wilson, M. & Monea, M. 2004. IEA GHG Weyburn CO_2 Monitoring & Storage Operation Summary Report 2000-2004. Petroleum Technology Research Centre, Regina.

[9] Kikuta, K., Hongo, S., Tanase, D. & Ohsumi, T, Field test of CO_2 injection in Nagaoka, Japan. In: Rubin, E.S., Keith, D.W. & Gilboy, C.F. (eds) Proceedings of the 7th International Conference on Greenhouse Gas Control Technologies, Volume 2 Contributed papers and panel discussion., Elsevier, Oxford, 2005, 1367–1372.

[10] Hovorka, S, Testing efficiency of CO2 storage in the subsurface: Frio Brine pilot project. In: Rubin, E.S., Keith, D.W. & Gilboy, C.F. (eds) Proceedings of the 7th International Conference on Greenhouse Gas Control Technologies,Volume 2. Contributed papers and panel discussion., Elsevier, Oxford, 2005, 1361–1366.

[11] Birkholzer, J.T., Zhou, Q., Tsang, C.-F, Large-scale Impact of CO_2 Storage in Deep Saline Aquifers: a Sensitivity Study on the Pressure Response in Stratified Systems, International Journal of Greenhouse Gas Control, 3(2), 2009, pp. 181-194.

[12] Zhou, Q., Birkholzer, J.T., Tsang, C.-F., Rutqvist, J., A method for quick assessment of CO2 storage capacity in closed and semi-closed saline formations. Int. J. Greenhouse Gas Control 2, 2008, 626–639.

[13] Kenneth E Peters, Alan E Cunningham, Clifford C Walters, Jiang Jigang and Fan Zhaon, Petroleum System in the Jiangling-Dangyang Area, Jianghan Basin, China, Geochem，24(10/11), 1996, 1035-1060.

[14] Liu Qiong, Sheng He, Zhen Lin Chen, Jian Feng Tian, Southwestern margin of Jianghan-Yuyang cretaceous sandstone basin: Reservoir Diagenesis and Pore Evolution, J Mineral Petrol， 27(2), 2007, 78-85 (in Chinese).

[15] Pruess, K., ECO2N: A TOUGH2 Fluid Property Module for Mixtures of Water, NaCl, and CO_2. Report LBNL-57952, 2005, Lawrence Berkeley National Laboratory, Berkeley, CA, USA.

[16] Pruess, K., Oldenburg, C.M., Moridis, G, TOUGH2 User's Guide, Version 2.0. Report LBNL-43134, 1999, Lawrence Berkeley National Laboratory, Berkeley, CA, USA.

[17] Yang, Y.L., Aplin, A.C., A permeability–porosity relationship for mudstones. Mar. Petrol. Geol. xxx, 2009, 1–6

[18] Neuzil, C.E, How permeable are clays and shales? Water Resour. Res. 30 (2), 1994, 145–150.

[19] Domenico, P.A., Schwartz, F.W., Physical and Chemical Hydrogeology, 2nd ed, 1998, John Wiley & Sons, Inc., New York.

[20] Hovorka, S.D., Doughty, C., Knox, P.R., Green, C.T., Pruess, K.,Benson, S.M, Evaluation of brine-bearing sands of the Frio formation, upper Texas gulf coast for geological sequestration of CO_2. In: First National Conference on Carbon Sequestration, National Energy Technology Laboratory, Pittsburgh, PA, USA, 14–17 May, 2001, p. 2001.

[21] Hart, D.J., Bradbury, K.R., Feinstein, D.T, The vertical hydraulic conductivity of an aquitard at two spatial scales. Ground Water 44 (2), 2006, 201–211.

[22] Fjaer, E., Holt, R.M., Horsrud, P., Raaen, A.M., Petroleum Related Rock Mechanics. Elsevier, Amsterdam, 1991.

[23] Hart, D.J, Laboratory Measurements of Poroelastic Constants and Flow Parameters and Some Associated Phenomena. Ph.D. Thesis. University of Wisconsin-Madison, Madison, WI, USA, 2000.

[24] Harris, J.M., Seismic Monitoring of CO_2 Sequestration. GCEP Technical Report. Stanford University, Palo Alto, CA, USA, 2006.

[25] Xie Taijun, Wu Lizhen, Jiang Jigang, Oil and Gas fields in the Jianghan Basin, Hubei Province, China, Wagner H C Wagner, L C , Wang F F H and Wong, F.L., editors, 1988, Petroleum resources of China and related subjects: Houston, Texas, Circum-Pacific Council for Energy and Mineral Resources Earth Sciences Series, 10, 1998,345-358